Solar Energy Materials & Solar Cells 149 (2016) 121–127

Contents lists available at ScienceDirect

Solar Energy Materials & Solar Cells

journal homepage: www.elsevier.com/locate/solmat

High-performance perovskite solar cells by incorporating a $ZnGa_2O_4$:Eu^{3+} nanophosphor in the mesoporous TiO_2 layer

Xian Hou [1], Tongtong Xuan [1], Hengchao Sun, Xiaohong Chen *, Huili Li **, Likun Pan ***

Engineering Research Center for Nanophotonics & Advanced Instrument, Ministry of Education, Department of Physics, East China Normal University, Shanghai 200062, China

ARTICLE INFO

Article history:
Received 23 September 2015
Received in revised form
3 December 2015
Accepted 19 January 2016

Keywords:
Perovskite solar cells
$ZnGa_2O_4$:Eu^{3+} nanophosphor
Power conversion efficiency

ABSTRACT

$ZnGa_2O_4$:Eu^{3+} nanophosphor was synthesized through a hydrothermal method and used as an effective light down-shifting/converting material in mesoporous TiO_2 layer of perovskite solar cells (PSCs). The nanophosphor can convert the high energy incident photon into the photon(s) with lower energy, which can excite $CH_3NH_3PbI_3$ to generate more photo generated electron–hole pairs, and thus promote the incident light use ratio and increase the power conversion efficiency (PCE) of PSCs. After the incorporation of suitable amount of $ZnGa_2O_4$:Eu^{3+} into PSCs, the cell PCE is increased to 13.80% with a photocurrent density of 23.68 mA cm^{-2} and a highest PCE of 14.34% with a photocurrent density of 25.02 mA cm^{-2} is achieved, much higher than those of the cell without $ZnGa_2O_4$:Eu^{3+} (PCE of 10.67% and photocurrent density of 20.2 mA cm^{-2}). The enhanced photovoltaic performance by incorporating the nanophosphor into PSCs should be ascribed to the increased incident light use ratio and improved exciton generation rate.

1. Introduction

As a newly emerging top research topic in solar cells, the hybrid inorganic–organic halide perovskite solar cells (PSCs) show great success and are viewed as "the next big thing" in photovoltaics [1–6], which is competitive with Cu(InGa)Se_2 [7–9], CdTe [10–13] or other kinds of thin film solar cells that have existed for decades. In PSCs, the perovskite layer acts as both the light absorber and charge transporter [14–21]. Although the widely used hybrid lead halide perovskite $CH_3NH_3PbI_3$ owns favorable direct bandgap (1.55 eV) for good light absorption in visible light spectrum, it cannot fully utilize the incident light within entire solar spectrum, especially ultraviolet (UV), near UV or infrared light, and hinders the efficient harvesting of photons, which is not beneficial to the improvement of power conversion efficiency (PCE) [22]. Therefore, an effective strategy to enhance the performance of PSCs lies in full utilization of the incident solar light [23].

In recent years, luminescent materials, which are capable of shifting or converting a broad spectrum of light into photon(s) of a particular wavelength [24,25]. Down-shifting is a single photon process that involves transformation of one absorbed high-energy photon into one lower-energy photon. This process obeys the Stokes Law with wavelength change known as the Stokes shift. Down-converting is able to split one incident high-energy photon into more than one lower-energy photons. Both of the processes could minimize the energy loss caused by thermalization of hot charge carriers after the absorption of high-energy photons [26,27]. Down-shifting/converting materials placed on the front side of light absorption layer have the potential to generate more suitable wavelength lights which can be absorbed well by photosensitive layer and they have been widely applied in conventional solar cells such as silicon solar cells [28–35], dye sensitized solar cells [36–44] and quantum dot-sensitized solar cells [45,46] to improve their light harvesting abilities. In our previous work, $Y_3Al_5O_{12}$:Ce [47] and $SrAl_2O_4$:Eu,Dy [45] phosphors were successfully used to enhance the light harvesting in sensitized solar cells by improving the light scattering and absorption. Such a method should be also helpful to improve the performance of PSCs. However, due to the large micron size of these bulk phosphors, they are difficult to be incorporated into any of the thin layers (thickness: 30–350 nm) within PSCs. Exploring nanosized luminescent materials with suitable emission wavelength which benefits the absorption of perovskite layer should be a promising method to solve this problem.

In this work, $ZnGa_2O_4$:Eu^{3+} nanophosphor was synthesized and incorporated into mesoporous TiO_2 layer of PSCs. The $ZnGa_2O_4$:Eu^{3+} nanophosphor acts as a light down-shifting/converting

* Corresponding author. Tel.: +86 21 62233676.
** Corresponding author. Tel.: +86 21 62235465.
*** Corresponding author. Tel.: +86 21 62234132; fax: +86 21 62234321.
E-mail addresses: xhchen@phy.ecnu.edu.cn (X. Chen), hlli@phy.ecnu.edu.cn (H. Li), lkpan@phy.ecnu.edu.cn (L. Pan).
[1] These authors contributed equally to this work.

http://dx.doi.org/10.1016/j.solmat.2016.01.021
0927-0248/

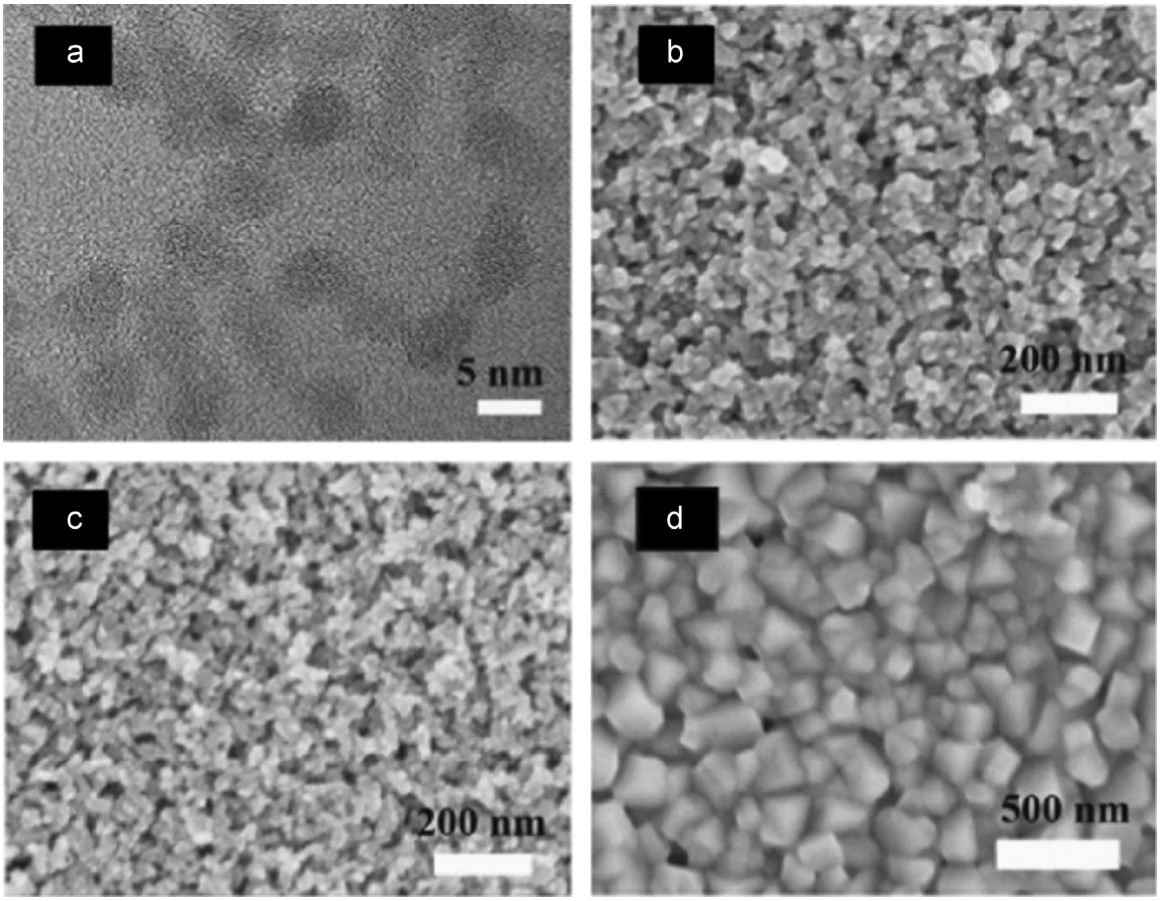

Fig. 1. (a) TEM image of $ZnGa_2O_4:Eu^{3+}$ nanophosphor; FESEM images of mesoporous TiO_2 layer (b) without and (c) with $ZnGa_2O_4:Eu^{3+}$ (8 mg ml^{-1}); (d) FESEM image of cuboid perovskite layer on (c).

material to absorb the high energy photons and emit lower energy photons that match the absorption of perovskite layer well, to generate more excited photo-generated electron–hole pairs. Therefore, the incident solar light can be taken advantages of more effectively. The PSCs with $ZnGa_2O_4:Eu^{3+}$ nanophosphor exhibit largely improved photocurrent density and PCE compared to those without $ZnGa_2O_4:Eu^{3+}$.

2. Materials and methods

2.1. Materials

All solvents and reagents were analytically pure and used as received. Fluorine-doped tin oxide (FTO) glass (thickness: 2.2 mm, resistivity: 14 Ω/□) was purchased from Nippon Sheet Glass, Japan. Lead(II) iodide (PbI_2, 99.9%), Lithium-bis(trifluoromethanesulfonyl) imide (Li-TFSI, 98%) and 4-tert-butylpyridine (TBP, 98%) were purchased from Aladdin Reagents. CH_3NH_3I was purchased from 1-Material-Organic Nano Electronic (1-Material Inc.). 2,2′,7,7′-tetrakis (N,N-di-p-methoxy-phenylamine)-9,9′-spirobifluorene (Spiro-OMe-TAD, ≥99%) was purchased from Banhe Technology Ltd., Changchun, China.

2.2. Synthesis of $ZnGa_2O_4:Eu^{3+}$

$ZnGa_2O_4:Eu^{3+}$ was synthesized through a hydrothermal method. 0.05 mmol $Zn(acac)_2$, 0.1 mmol $Ga(acac)_3$, 0.01 mmol Eu $(acac)_3$ and 20 ml oleylamine were added into 50 ml flask. The solution was heated at 120 °C under vacuum for 30 min and at 300 °C under N_2 atmosphere for 6 h. The product was isolated by centrifugation, washed using chloroform and methanol, and dried under vacuum overnight. The color of obtained $ZnGa_2O_4:Eu^{3+}$ nanophosphor is tan.

2.3. Fabrication of PSCs

FTO was patterned by etching using zinc powder and 2 M hydrochloric acid. The substrates were ultrasonically cleaned using deionized water, isopropanol and ethanol, and then treated under UV-ozone for 15 min to remove the organic residue. Compact TiO_2 layer was prepared by spin-coating of TiO_2-sol on patterned FTO glass at 4000 rpm for 60 s and sintered at 500 °C for 30 min. Subsequently, the diluted TiO_2 pastes (Dyesol 18NR-T, 1:3.5 mass ratio with ethanol) with different amount of well-dispersed $ZnGa_2O_4:Eu^{3+}$ nanophosphors (6 mg ml^{-1}, 8 mg ml^{-1}, 10 mg ml^{-1}) were spin coated on the compact TiO_2 layer at 3000 rpm for 60 s as mesoporous layer and the obtained corresponding PSCs were labeled as ZGO-6, ZGO-8 and ZGO-10, respectively. The as-prepared electrodes were dried at 100 °C for 5 min and sintered at 500 °C for 30 min. Finally the substrates were immersed in 40 mM $TiCl_4$ aqueous solutions for 30 min at 70 °C and washed with deionized water and ethanol, followed by annealing at 500 °C for 30 min in air. The equally thick mesoporous layer without $ZnGa_2O_4:Eu^{3+}$ was also prepared as control sample for comparison.

$CH_3NH_3PbI_3$ was formed using typical two-step spin-coating procedure under argon atmosphere. 1 M PbI_2 solution was prepared by dissolving 462 mg PbI_2 in 1 ml N,N-dimethylformamide (DMF, 99.8%, Aladdin) under stirring at 70 °C overnight. 20 μl PbI_2

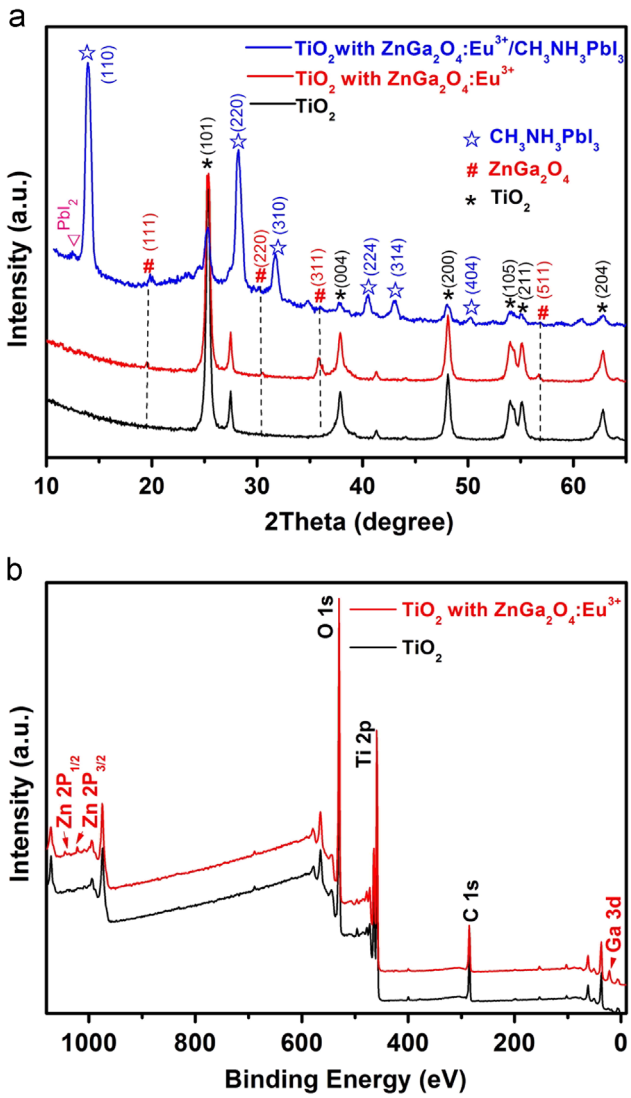

Fig. 2. (a) XRD patterns of mesoporous TiO_2 without (black curve) and with $ZnGa_2O_4$:Eu^{3+} (red curve, 8 mg ml^{-1}) and TiO_2 with $ZnGa_2O_4$:Eu^{3+}(8 mg ml^{-1})/ $CH_3NH_3PbI_3$ (blue curve); (b) XPS spectra of mesoporous TiO_2 without (black curve) and with (red curve) $ZnGa_2O_4$:Eu^{3+} (8 mg ml^{-1}). (For interpretation of the references to color in this figure legend, the reader is referred to the web version of this article.)

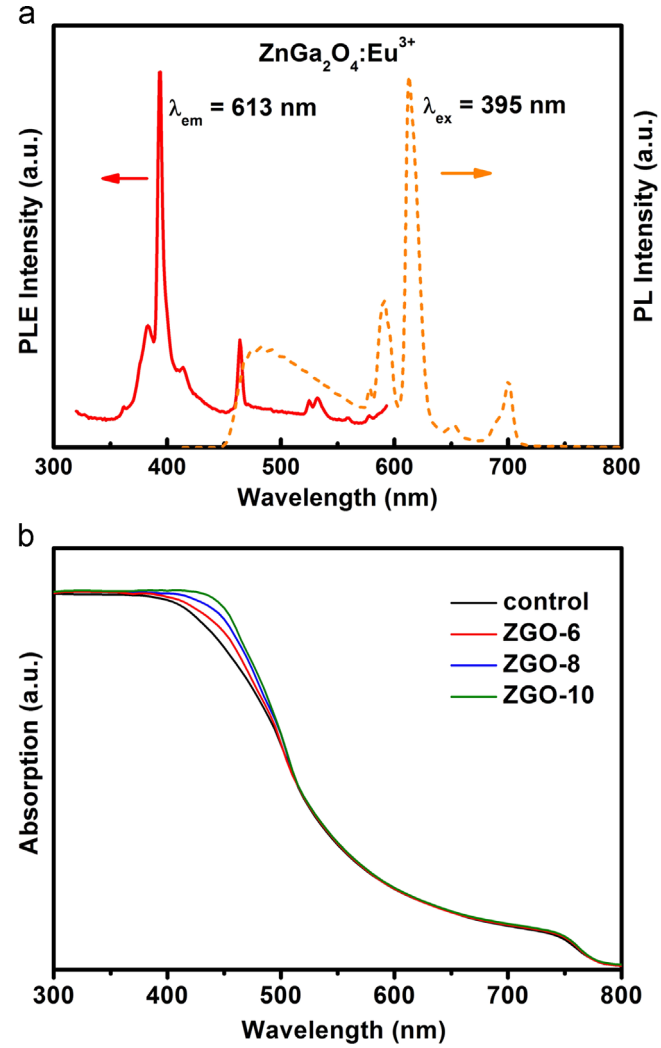

Fig. 3. (a) PL excitation and emission spectra of $ZnGa_2O_4$:Eu^{3+} nanophosphor. (b) UV–vis absorption spectra of mesoporous TiO_2/$CH_3NH_3PbI_3$ (control) and TiO_2 with different amounts of $ZnGa_2O_4$:Eu^{3+}/$CH_3NH_3PbI_3$ (ZGO-6, ZGO-8 and ZGO-10).

solution was spin-coated on the mesoporous layer at 3000 rpm for 5 s and 6000 rpm for 5 s. After that, the film was dried at 40 °C for 3 min and then at 90 °C for 5 min. 200 μl CH_3NH_3I solution in 2-propanol (8 mg ml^{-1}) was dropped on the PbI_2-coated substrate for 30 s, spun at 4000 rpm for 30 s and dried at 95 °C for 30 min to form $CH_3NH_3PbI_3$ perovskite layer. Subsequently, 72.3 mg Spiro-OMeTAD, 28.8 μl TBP and 17.5 μl Li-TFSI acetonitrile solution (520 mg ml^{-1}) were dissolved in 1 ml chlorobenzene and then 20 μl of the above solution was put on the $CH_3NH_3PbI_3$ perovskite layer by spin coating at 5000 rpm for 60 s to form Spiro-OMeTAD based hole transfer layer. Finally, 80 nm thick Ag/Al electrode with an active area of 0.1 cm^2 was evaporated on the Spiro-OMeTAD-coated film.

2.4. Characterization

The morphology, structure and composition of the samples were investigated by field-emission scanning electron microscopy (FESEM, Hitachi S-4800), transmission electron microscopy (TEM, JEOL-2100), X-ray diffraction (XRD, Holland Panalytical PRO PW3040/60) with Cu Kα radiation (V=30 kV, I=25 mA), and X-ray photoelectron spectroscopy (XPS, Thermo ESCALAB 250XI) using Al-Kα monochromatic radiation. UV–vis absorption spectra were detected using a UV–vis spectrophotometer (Hitachi U-3900). Photoluminescence (PL) spectra were examined using a fluorescence spectrophotometer (HORIBA Jobin Yvon Fluoromax-4). The photocurrent density–voltage (J–V) curve was measured using a Keithley model 2440 Source Meter under the illumination of simulated AM 1.5 G solar light from a Newport solar simulator system (equipped with a 1 kW Xenon arc lamp, Oriel, calibrated with a standard silicon reference cell). The solar cells were masked with a black aperture to define the active area of 0.1 cm^2. The incident photon to current conversion efficiency (IPCE) was measured as a function of wavelength ranging from 300 to 800 nm using a Newport Optical Power Meter 2936-R controlled by TracQ Basic software.

3. Results and discussion

Fig. 1(a) gives the TEM image of $ZnGa_2O_4$:$Eu^{3+}$and it shows regular spherical nanoparticle shape with a size of about 5 nm. Fig. 1(b) and (c) displays the FESEM images of mesoporous TiO_2 layer without and with $ZnGa_2O_4$:Eu^{3+} nanophosphor, respectively.

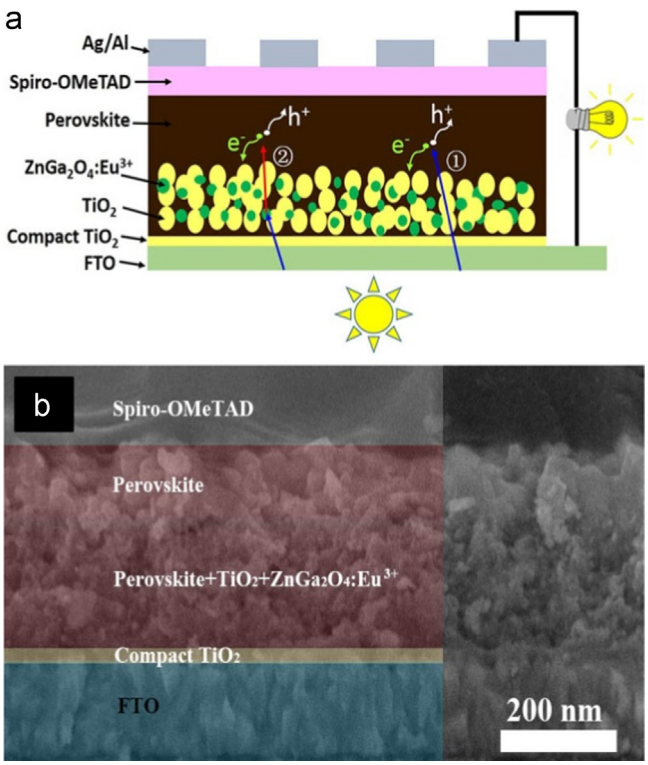

Fig. 4. Schematic structure (a) and cross section SEM image (b) of the PSCs with $ZnGa_2O_4:Eu^{3+}$.

Table 1
Photovoltaic parameters of control cell and ZGO-6, ZGO-8 and ZGO-10.

Sample	V_{oc} (V)	J_{sc} (mA cm^{-2})	FF (%)	η (%)	R_s (Ω cm^{-2})	R_{sh} (Ω cm^{-2})
control	0.93	20.12	57	10.67	74.16	5410.89
ZGO-6	0.94	22.98	59	12.74	75.40	5404.56
ZGO-8	0.94	23.68	62	13.80	75.92	5399.34
ZGO-10	0.93	22.06	58	11.90	77.08	5315.68

Due to the small size of $ZnGa_2O_4:Eu^{3+}$, the morphology of mesoporous layer is almost not changed after the incorporation of $ZnGa_2O_4:Eu^{3+}$. An uniform and compact cubic $CH_3NH_3PbI_3$ perovskite layer on mesoporous layer prepared by typical two-step spin-coating procedure is observed from Fig. 1(d), which is beneficial to the electron transfer for improving the cell performance [48]. It also indicates that the incorporated $ZnGa_2O_4:Eu^{3+}$ nanophosphor does not affect the crystallization of $CH_3NH_3PbI_3$.

Fig. 2(a) shows XRD patterns of TiO_2, TiO_2 with $ZnGa_2O_4:Eu^{3+}$ and TiO_2 with $ZnGa_2O_4:Eu^{3+}/CH_3NH_3PbI_3$. The small peaks in patterns of TiO_2 with $ZnGa_2O_4:Eu^{3+}$ and TiO_2 with $ZnGa_2O_4:Eu^{3+}/CH_3NH_3PbI_3$ at 19.7°, 30.3°, 35.7° and 57.4° correspond to (111), (220), (311), and (511) planes of $ZnGa_2O_4$ (JCPDF No. 86-0415), which proves the existence of $ZnGa_2O_4:Eu^{3+}$ in the mesoporous layer. The strong peaks at 14.08°, 28.41° and 31.85° for $CH_3NH_3PbI_3$ coated sample are assigned to (110), (220) and (310) planes of $CH_3NH_3PbI_3$ [49], indicating an orthorhombic crystal structure of halide perovskite with high crystallinity. The weak peak at 12.65° should be ascribed to a low-level impurity of PbI_2 [50]. The existence of $ZnGa_2O_4:Eu^{3+}$ was further confirmed by XPS, as shown in Fig. 2(b), from which the peaks of Ga 3d, O 1s, Zn $2p_{1/2}$ and Zn $2p_{3/2}$ are found. However, due to the low content of Eu in $ZnGa_2O_4:Eu^{3+}$, Eu signal is not found.

Fig. 3(a) gives PL excitation and emission spectra of $ZnGa_2O_4:Eu^{3+}$ nanophosphor. The sharp peaks extended from 360 to 540 nm are ascribed to f–f transition of Eu^{3+} from the fundamental $^7F_0$ state to different excited states. The emission spectra consist of sharp peaks ranging from 450 to 720 nm, which are associated with the intrinsic $ZnGa_2O_4$ emission and the transitions from excited $^5D_0$ level to ^7F_J (J=1; 2; 3; 4) levels of Eu^{3+} [51,52]. The correlation between the narrow lines of the PL spectra and the XRD patterns confirms that the Eu^{3+} ion is incorporated into the host matrix [53]. The emitted light with longer wavelength can be absorbed by the perovskite layer with narrow bandgap (1.55 eV) better and thus the light harvesting is enhanced. Fig. 3(b) displays the UV–vis absorption spectra of $TiO_2/CH_3NH_3PbI_3$ and TiO_2 with $ZnGa_2O_4:Eu^{3+}/CH_3NH_3PbI_3$. It should be noticed that the samples with nanophosphor show stronger absorption from 380 to 500 nm than that without nanophosphor and the UV absorption becomes more intense with the increase in the content of nanophosphor.

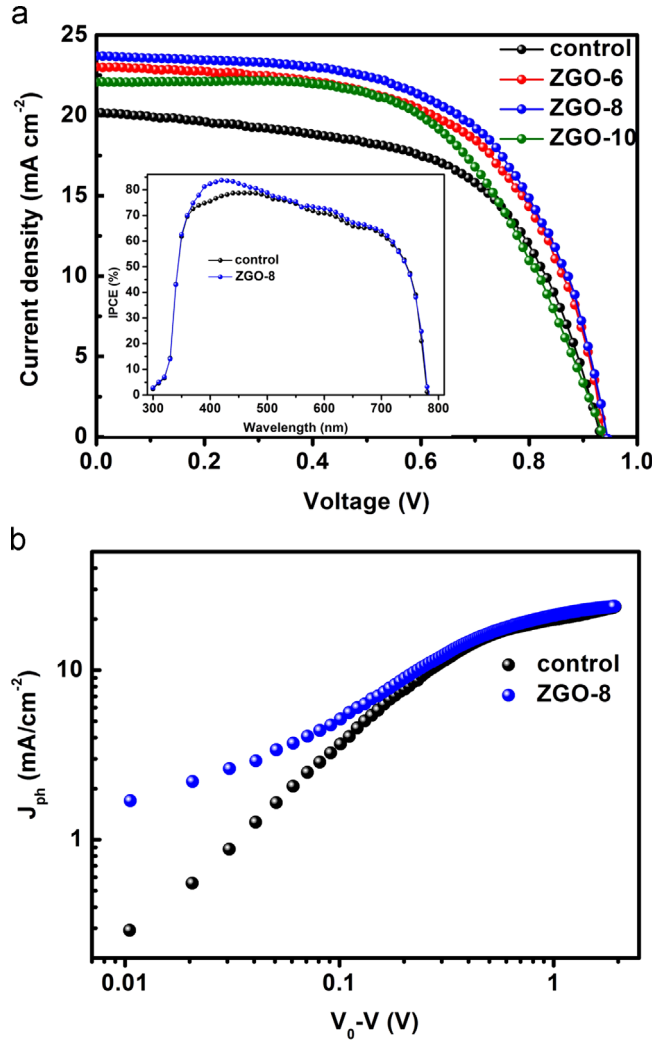

Fig. 5. (a) J–V curves of control cell, ZGO-6, ZGO-8 and ZGO-10. The inset is the IPCE spectra of control cell and ZGO-8. (b) Double logarithmic plot of photocurrent ($J_{ph}=J_{light}-J_{dark}$) versus effective applied voltage (V_0–V) for control cell and ZGO-8.

The schematic structure and cross section FESEM image of the PSCs with $ZnGa_2O_4:Eu^{3+}$ are displayed in Fig. 4(a) and (b), respectively. When the light enters into in solar cells from FTO side, some photons go through directly and are absorbed by perovskite layer, while part of high energy photons are transferred to low energy photons by $ZnGa_2O_4:Eu^{3+}$ to be absorbed by perovskite better, which can reduce the energy loss caused by thermalization of hot charge carriers after the absorption of high-energy photons [27]. Such a phenomenon can be observed from

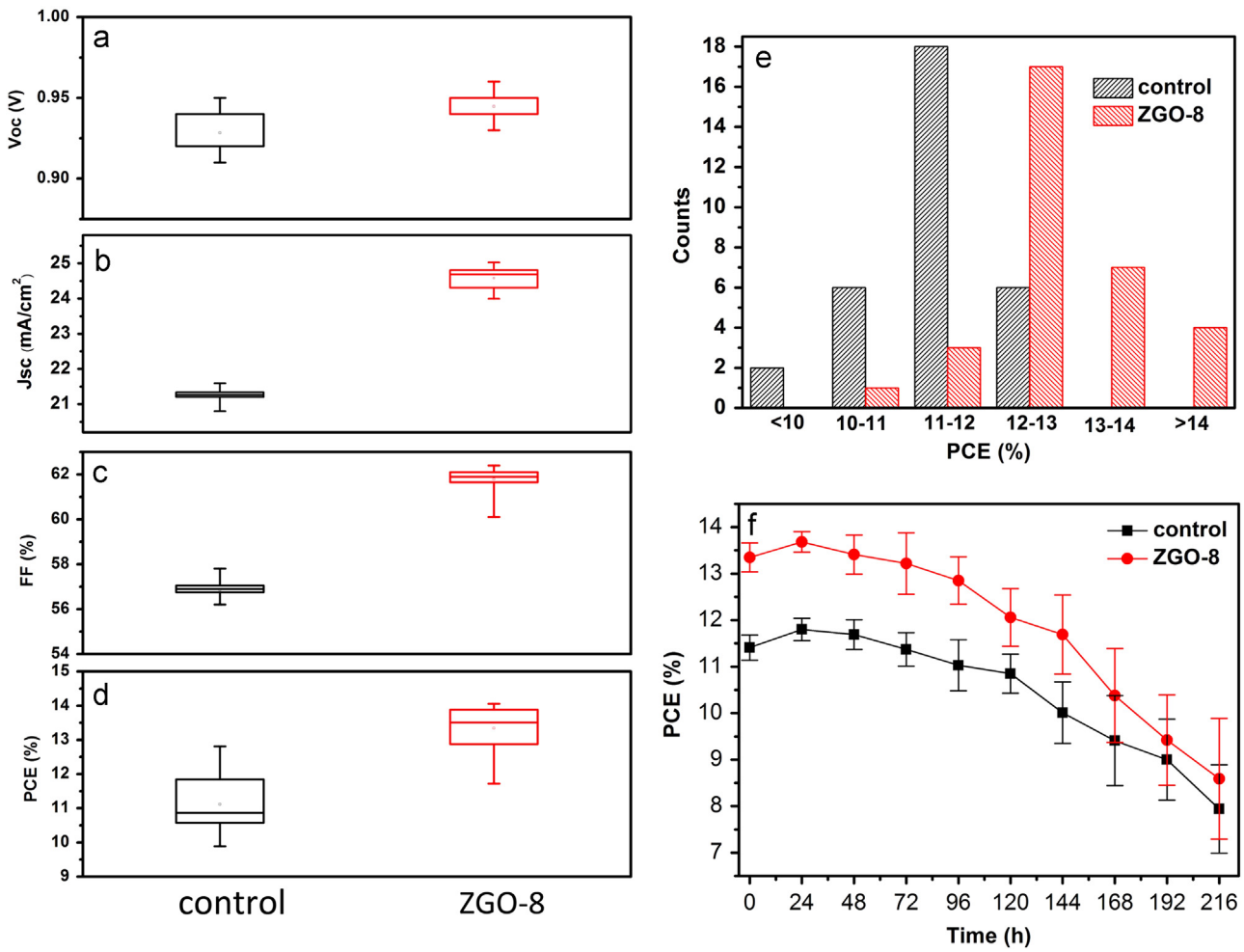

Fig. 6. Photovoltaic parameter distributions of 32 control cells and 32 ZGO-8 cells: (a) open circuit voltage, (b) short circuit current, (c) fill factor and (d) PCE. (e) Histograms of PCE measured for each 32 separate cells. (f) PCE plotted as a function of storage time for control cells (black squares) and ZGO-8 cells (red circles). Measurements were made on at least 32 cells of each type, and the error bars represent plus or minus one standard deviation from the mean. (For interpretation of the references to color in this figure legend, the reader is referred to the web version of this article.)

UV–vis spectra of $TiO_2/CH_3NH_3PbI_3$ and TiO_2 with $ZnGa_2O_4:Eu^{3+}/CH_3NH_3PbI_3$ in Fig. 3(b).

After spin-coating Spiro-OMeTAD based hole transfer materials and evaporating Ag/Al electrode on the perovskite layer, the *J–V* character was measured using a Keithley model 2440 Source Meter under the illumination of simulated AM 1.5 G solar light from a Newport solar simulator system. The photovoltaic parameters of the cells are summarized in Table 1 and the corresponding *J–V* curves are displayed in Fig. 5(a). It can be found that the control cell shows a PCE of 10.67% and the efficiency is gradually increased with the increase in the content of $ZnGa_2O_4:Eu^{3+}$ and the ZGO-8 cell shows a highest PCE of 13.80%. The corresponding current density is enhanced from 20.12 to 23.68 mA cm^{-2} due to the improvement of light absorption. The FF is also increased slightly from 57% to 62%. The increase of current density and FF by incorporating the $ZnGa_2O_4$ has been observed in dye-sensitized solar cells by Kim et al. [54]. However, when the content of $ZnGa_2O_4:Eu^{3+}$ is further increased (ZGO-10), the cell performance deteriorates, which should be ascribed to the increase of the cell resistance (R_s) by incorporating excessive nanophosphor [55], as shown in Table 1.

To further understand the mechanism responsible for the enhanced performance by incorporating nanophosphor, the exciton generation rates in ZGO-8 cell and control cell were investigated. Fig. 5(b) shows the photocurrent density (J_{ph}) of two devices. J_{ph} is determined by the equation $J_{ph}=J_{light}-J_{dark}$, where J_{light} and J_{dark} are the current densities measured under one sun illumination and in dark condition, respectively. The plot of J_{ph} with respect to the effective voltage (V_0–V), where V_0 is the compensation voltage (defined by the voltage at which $J_{ph}=0$) [56,57] and V is the applied voltage, demonstrates two regions. Noticeably, in low effective voltage (<0.3 V), the photocurrents in two devices increase sharply with the increase in effective voltage, and in higher effective voltage, the photocurrents reach gradually a saturated value. From Fig. 5(b), it can be seen that ZGO-8 exhibits a larger saturated photocurrent than control cell. In general, the saturated photocurrent correlates to the maximum exciton generation rate (G_{max}), which is mainly governed by the light absorption [55,57]. The higher exciton generation rate should contribute to higher FF of ZGO-8 than control cell. Therefore, the improved J_{ph} further confirms that the incorporated nanophosphor into PSCs enhances the light harvesting in the device.

The photovoltaic parameter distributions of 32 ZGO-8 cells and 32 control cells are statistically summarized in Fig. 6(a)–(e). Clearly, the cell efficiency is significantly improved with the proper introduction of $ZnGa_2O_4:Eu^{3+}$ nanophosphor mainly by improving the photocurrent density. From Fig. 6(e), both of the control cells and ZGO-8 cells show narrow PCE distribution, indicating that the errors from our preparation and testing are small and the improvement of PCE should come from the enhanced light

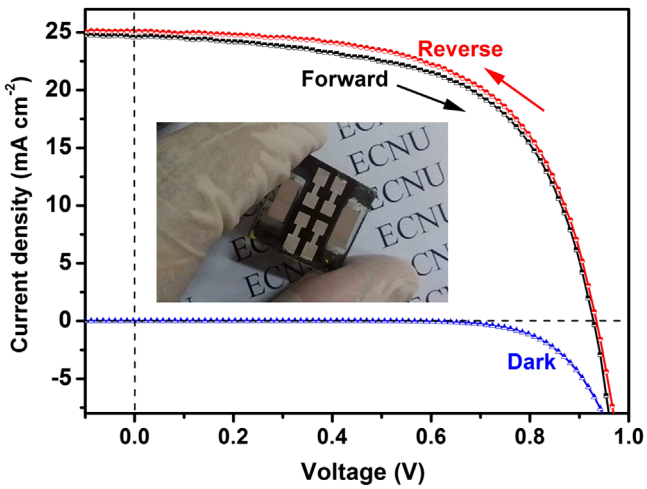

Fig. 7. *J–V* curves of best performance ZGO-8 cell. The black curve was measured at forward scan, the red at reverse scan, and the blue curveat dark. The inset is photograph of corresponding cell (substrate size: 2.5 cm × 2.5 cm). (For interpretation of the references to color in this figure legend, the reader is referred to the web version of this article.)

harvesting contributed by $ZnGa_2O_4$:Eu^{3+}. The IPCE spectrum of ZGO-8 exhibits a maximum value of 84% at 420 nm, while for the cell without $ZnGa_2O_4$:Eu^{3+}, the peak only reaches 77%, as shown in the inset of Fig. 5(a). Such an obvious increase of IPCE value in the range from 380 to 490 nm for ZGO-8 cell should be ascribed to the light down-shifting/converting by $ZnGa_2O_4$:Eu^{3+} nanophosphor, which matches the UV–vis absorption measurement result well. The contribution of light scattering by the microsized phosphors reported in our pervious works [45–47] can be ignored here because the light-scattering effects of very small 5 nm $ZnGa_2O_4$:Eu^{3+} nanoparticles are often minimal [58]. The ZGO-8 cell displays a best performance with a V_{oc} of 0.94 V, a J_{sc} of 25.02 mA cm^{-2} and a FF of 61%, yielding a PCE of 14.34% under AM 1.5 G, 100 mW cm^{-2} light illumination, as shown in Fig. 7.The hysteresis of the ZGO-8 cell with best performance was further studied. Due to the uniform and compact perovskite layer with large grain size, as confirmed by FESEM measurement, forward scan (black curve) and reverse scan (red curve) in Fig. 7 show a slight difference, which suggests that the hysteresis phenomenon in this cell is very small.

Moreover, the stability of the cells was tested by storing them in ambient air (relative humidity 40–45%; temperature 21–23 °C) and dark conditions. The ZGO-8 cells and the control cells maintain 66% and 70%of their initial efficiencies over 9 days, respectively, as shown in Fig. 6(f).

4. Conclusion

$ZnGa_2O_4$:Eu^{3+} nanophosphor was successfully synthesized and introduced into mesoporous TiO_2 layer of PSCs. A highest PCE of 14.34% and a typical PCE of 13.80% under one sun illumination is achieved, much higher than that of the cell without $ZnGa_2O_4$:Eu^{3+}. The large improvement of PCE is attributed to the enhanced light harvesting mainly via the light down-shifting/converting offered by the $ZnGa_2O_4$:Eu^{3+} nanophosphor and improved exciton generation rate. Especially, a high photocurrent density of 25.02 mA cm^{-2} is obtained, indicating that the incorporation of $ZnGa_2O_4$:Eu^{3+} nanophosphor should be an effective method to improve the performance of PSCs.

Acknowledgments

This work is supported by the National Natural Science Foundation of China (NSFC) (61275038, 51472087) and the ECNU Reward for Excellent Doctoral Students in Academics (xrzz2014029).

References

[1] H. Zhou, Q. Chen, G. Li, S. Luo, T.B. Song, H.S. Duan, Z. Hong, J. You, Y. Liu, Y. Yang, Interface engineering of highly efficient perovskite solar cells, Science 354 (2014) 542–546.
[2] J.M. Ball, M.M. Lee, A. Hey, H.J. Snaith, Low-temperature processed meso-superstructured to thin-film perovskite solar cells, Energy Environ. Sci. 6 (2013) 1739–1743.
[3] B. Cai, Y. Xing, Z. Yang, W.H. Zhang, J. Qiu, High performance hybrid solar cells sensitized by organolead halide perovskites, Energy Environ. Sci. 6 (2013) 1480–1485.
[4] Q. Wang, Y. Shao, Q. Dong, Z. Xiao, Y. Yuan, J. Huang, Large fill-factor bilayer iodine perovskite solar cells fabricated by a low-temperature solution-process, Energy Environ. Sci. 7 (2014) 2359–2365.
[5] C. Zuo, L. Ding, An 80.11% FF record achieved for perovskite solar cells by using the NH_4Cl additive, Nanoscale 6 (2014) 9935–9938.
[6] S. Lv, L. Han, J. Xiao, L. Zhu, J. Shi, H. Wei, Y. Xu, J. Dong, X. Xu, D. Li, S. Wang, Y. Luo, Q. Meng, X. Li, Mesoscopic $TiO_2/CH_3NH_3PbI_3$ perovskite solar cells with new hole-transporting materials containing butadiene derivatives, Chem. Commun. 50 (2014) 6931–6934.
[7] P. Jackson, D. Hariskos, R. Wuerz, W. Wischmann, M. Powalla, Compositional investigation of potassium doped Cu(In, Ga)Se_2 solar cells with efficiencies up to 20.8%, Phys Status Solidi RRL 8 (2014) 219–222.
[8] P. Jackson, D. Hariskos, E. Lotter, S. Paetel, R. Wuerz, R. Menner, W. Wischmann, M. Powalla, New world record efficiency for Cu(In, Ga)Se_2 thin-film solar cells beyond 20%, Prog. Photovolt. 19 (2011) 894–897.
[9] P. Reinhard, A. Chirila, P. Blosch, F. Pianezzi, S. Nishiwaki, S. Buecheler, A. N. Tiwari, Review of progress toward 20% efficiency flexible CIGS solar cells and manufacturing issues of solar modules, IEEE J. Photovolt. 3 (2013) 572–580.
[10] J. Britt, C. Ferekides, Thin-film CdS/CdTe solar cell with 15.8% efficiency, Appl. Phys. Lett. 62 (1993) 2851 2582.
[11] A. Gupta, V. Parikh, A.D. Compaan, High efficiency ultra-thin sputtered CdTe solar cells, Sol. Energy Mater. Sol. Cells 90 (2006) 2263–2271.
[12] A. Romeo, G. Khrypunov, F. Kurdesau, M. Arnold, D.L. Bätzner, H. Zogg, A. N. Tiwari, High-efficiency flexible CdTe solar cells on polymer substrates, Sol. Energy Mater. Sol. Cells 90 (2006) 3407–3415.
[13] M. Gloeckler, I. Sankin, Z. Zhao, CdTe solar cells at the threshold to 20% efficiency, IEEE J. Photovolt. 3 (2013) 1389–1393.
[14] W.A. Laban, L. Etgar, Depleted hole conductor-free lead halide iodide heterojunction solar cells, Energy Environ. Sci. 6 (2013) 3249–3253.
[15] C. Sun, Y. Guo, H. Duan, Y. Chen, Y. Guo, H. Li, H. Liu, Solvent-assisted growth of organic–inorganic hybrid perovskites with enhanced photovoltaic performances, Sol. Energy Mater. Sol. Cells 143 (2015) 360–368.
[16] J. You, Z. Hong, Y.M. Yang, Q. Chen, M. Cai, T.B. Song, C.C. Chen, S. Lu, Y. Liu, H. Zhou, Y. Yang, Low-temperature solution-processed perovskite solar cells with high efficiency and flexibility, ACS Nano 8 (2014) 1674–1680.
[17] V. GonzalezPedro, E.J. JuarezPerez, W.S. Arsyad, E.M. Barea, F. Fabregat Santiago, I. MoraSero, J. Bisquert, General working principles of $CH_3NH_3PbX_3$ perovskite solar cells, Nano Lett. 14 (2014) 888–893.
[18] J. Seo, S. Park, Y. Chan Kim, N.J. Jeon, J.H. Noh, S.C. Yoon, S.I. Seok, Benefits of very thin PCBM and LiF layers for solution-processed p-i-n perovskite solar cells, Energy Environ. Sci. 7 (2014) 2642–2646.
[19] H.S. Jung, N.G. Park, Perovskite solar cells: from materials to devices, Small 11 (2015) 10–25.
[20] W.J. Yin, T. Shi, Y. Yan, Unique properties of halide perovskites as possible origins of the superior solar cell performance, Adv. Mater. 26 (2014) 4653–4658.
[21] J.W. Lee, T.Y. Lee, P.J. Yoo, M. Grätzel, S. Mhaisalkar, N.G. Park, Rutile TiO_2-based perovskite solar cells, J. Mater. Chem. A 2 (2014) 9251–9259.
[22] N.G. Park, Perovskite solar cells: an emerging photovoltaic technology, Mater. Today 18 (2015) 65–72.
[23] A. Kojima, K. Teshima, Y. Shirai, T. Miyasaka, Organometal halide perovskites as visible-light sensitizers for photovoltaic cells, J. Am. Chem. Soc. 131 (2009) 6050–6051.
[24] Q. Shi, J. Zhang, C. Cai, L. Cong, T. Wang, Synthesis and photoluminescent properties of Eu^{3+}-doped $ZnGa_2O_4$ nanophosphors, Mater. Sci. Eng. B 149 (2008) 82–86.
[25] J. Liu, X. Wang, T. Xuan, H. Li, Z. Sun, Photoluminescence, thermal stability of Mn^{2+} co-doped $SrSi_2O_2N_2$:Eu^{2+} green phosphor synthesized by sol–gel method, J. Alloy. Compd., 593, (2014) 128–131.
[26] Q.Y. Zhang, X.Y. Huang, Recent progress in quantum cutting phosphors, Prog. Mater. Sci. 55 (2010) 353–427.
[27] X.Y. Huang, S.Y. Han, W. Huang, X.G. Liu, Enhancing solar cell efficiency: the search for luminescent materials as spectral converters, Chem. Soc. Rev. 42 (2013) 173–201.

[28] A. Shalav, B.S. Richards, T. Trupke, K.W. Krämer, H.U. Güdel, Application of $NaYF_4$: Er^{3+} up-converting phosphors for enhanced near-infrared silicon solar cell response, Appl. Phys. Lett., 86, (2005) 013505.
[29] T. Trupke, A. Shalav, B.S. Richards, P. Würfel, M.A. Green, Efficiency enhancement of solar cells by luminescent up-conversion of sunlight, Sol. Energy Mater. Sol. Cells 90 (2006) 3327–3338.
[30] B.S. Richards, Luminescent layers for enhanced silicon solar cell performance: Down-conversion, Sol. Energy Mater. Sol. Cells 90 (2006) 1189–1207.
[31] J. de Wild, A. Meijerink, J.K. Rath, W.G.J.H.M. van Sark, R.E.I. Schropp, Up converter solar cells: materials and applications, Energy Environ. Sci. 4 (2011) 4835–4848.
[32] J. de Wild, A. Meijerink, J.K. Rath, W.G.J.H.M. van Sark, R.E.I. Schropp, Towards up conversion for amorphous silicon solar cells, Sol. Energy Mater. Sol. Cells 94 (2010) 1919–1922.
[33] Y.C. Chen, T.M. Chen, Improvement of conversion efficiency of silicon solar cells using up-conversion molybdate $La_2Mo_2O_9$:Yb, R (R=Er, Ho) phosphors, J. Rare Earth 29 (2011) 723–726.
[34] Y.Y. Cheng, B. Fückel, R.W. MacQueen, T. Khoury, R.G.C.R. Clady, T.F. Schulze, N. J. EkinsDaukes, M.J. Crossley, B. Stannowski, K. Lips, T.W. Schmidt, Improving the light-harvesting of amorphous silicon solar cells with photochemical upconversion, Energy Environ. Sci. 5 (2012) 6953–6959.
[35] Q. Zhang, J. Wang, G. Zhang, Q. Su, UV photon harvesting and enhanced near-infrared emission in novel quantum cutting Ca_2BO_3Cl:Ce^{3+}, Tb^{3+}, Yb^{3+} phosphor, J. Mater. Chem. 19 (2009) 7088–7092.
[36] X.Y. Huang, J.X. Wang, D.C. Yu, S. Ye, Q.Y. Zhang, X.W. Sun, Spectral conversion for solar cell efficiency enhancement using YVO_4:Bi^{3+}, Ln^{3+} (Ln=Dy, Er, Ho, Eu, Sm, and Yb) phosphors, J. Appl. Phys. 109 (2011) 113526.
[37] W. He, T.S. Atabaev, H.K. Kim, Y.H. Hwang, Enhanced sunlight harvesting of dye-sensitized solar cells assisted with long persistent phosphor materials, J. Phys. Chem. C 117 (2013) 17894–17900.
[38] M.J. Lim, Y.N. Ko, Y. Chan Kang, K.Y. Jung, Enhancement of light-harvesting efficiency of dye-sensitized solar cells via forming TiO_2 composite double layers with down/up converting phosphor dispersion, RSC Adv. 4 (2014) 10039–10042.
[39] J. Dewalque, R. Cloots, F. Mathis, O. Dubreuil, N. Krins, C. Henrist, TiO_2 multilayer thick films (up to 4 μm) with ordered mesoporosity: influence of template on the film mesostructure and use as high efficiency photoelectrode in DSSCs, J. Mater. Chem. 21 (2011) 7356–7363.
[40] S.G. Shin, K.H. Kim, C.W. Bark, H.W. Choi, Preparation of a Phosphor/TiO_2 nanoparticle composite layer for applications in dye-sensitized solar cells, J. Korean Phys. Soc. 65 (2014) 387–391.
[41] C.W. Kim, D.K. Kim, W.J. Shin, M.J. Choi, Y.S. Kang, Y.S. Kang, Phosphor positioning for effective wavelength conversion in dye-sensitized solar cells, Nano Energy 13 (2015) 573–581.
[42] X. Huang, S. Han, W. Huang, X. Liu, Enhancing solar cell efficiency: the search for luminescent materials as spectral converters, Chem. Soc. Rev. 42 (2013) 173–201.
[43] Y. Li, G. Wang, K. Pan, B. Jiang, C. Tian, W. Zhou, H. Fu, $NaYF_4$:Er^{3+}/Yb^{3+}-graphene composites: preparation, upconversion luminescence, and application in dye-sensitized solar cells, J. Mater. Chem. 22 (2012) 20381–20386.
[44] J. Bai, R. Zhao, G. Han, Z. Li, G. Diao, Synthesis of 1D upconversion CeO_2:Er, Yb nanofibers via electrospinning and their performance in dye-sensitized solar cells, RSC Adv. 5 (2015) 43328–43333.
[45] H.C. Sun, L.K. Pan, X.Q. Piao, Z. Sun, Long afterglow $SrAl_2O_4$:Eu, Dy phosphors for CdS quantum dot-sensitized solar cells with enhanced photovoltaic performance, J. Mater. Chem. A 1 (2013) 6388–6392.
[46] H.C. Sun, L.K. Pan, G. Zhu, X.Q. Piao, L. Zhang, Z. Sun, Long afterglow $Sr_4Al_{14}O_{25}$:Eu, Dy phosphors as both scattering and down converting layer for CdS quantum dot-sensitized solar cells, Dalton Trans. 43 (2014) 14936–14941.
[47] G. Zhu, X.J. Wang, H.L. Li, L.K. Pan, H.C. Sun, X.J. Liu, T. Lv, Z. Sun, $Y_3Al_5O_{12}$:Ce phosphors as a scattering layer for high-efficiency dye sensitized solar cells, Chem. Commun. 48 (2012) 958–960.
[48] J.H. Im, I.H. Jang, N. Pellet, M. Grätzel, N.G. Park, Growth of $CH_3NH_3PbI_3$ cuboids with controlled size for high-efficiency perovskite solar cells, Nat. Nanotechnol. 9 (2014) 927–932.
[49] Q. Chen, H. Zhou, Z. Hong, S. Luo, H.S. Duan, H.H. Wang, Y. Liu, G. Li, Y. Yang, Planar heterojunction perovskite solar cells via vapor-assisted solution process, J. Am. Chem. Soc. 136 (2014) 622–625.
[50] M. Liu, M.B. Johnston, H.J. Snaith, Efficient planar heterojunction perovskite solar cells by vapour deposition, Nature 501 (2013) 395–398.
[51] J. Su Kim, A. Kyung Kwon, J.S. Kim, H. Lee Park, G. Chul Kim, S. do Han, Optical and structural properties of $ZnGa_2O_4$:Eu^{3+} nanophosphor by hydrothermal method, J. Lumin., 122, (2007) 851–854.
[52] S. Seo, H. Yang, P.H. Holloway, Synthesis and properties of colloidal ternary $ZnGa_2O_4$:Eu^{3+} nanocrystals, J. Lumin., 129, (2009) 307–311.
[53] E. Rusu, V. Ursaki, G. Novitschi, M. Vasile, P. Petrenco, L. Kulyuk, Luminescence properties of $ZnGa_2O_4$ and $ZnAl_2O_4$ spinels doped with Eu^{3+} and Tb^{3+} ions, Phys. Status Solidi C 6 (2009) 1199–1202.
[54] Y.M. Kim, K.H. Kim, C.W. Bark, H.W. Choi, Enhancing performance of dye-sensitized solar cell influenced by phosphor $ZnGa_2O_4$, Mol. Cryst. Liq. Cryst. 598 (2014) 40–46.
[55] M.F. Xu, X.Z. Zhu, X.B. Shi, J. Liang, Y. Jin, Z.K. Wang, L.S. Liao, Plasmon resonance enhanced optical absorption in inverted polymer/fullerene solar cells with metal nanoparticle-doped solution-processable TiO_2 layer, ACS Appl. Mater. Interfaces 5 (2013) 2935–2942.
[56] F.C. Chen, J.L. Wu, C.L. Lee, Y. Hong, C.H. Kuo, M.H. Huang, Plasmonic-enhanced polymer photovoltaic devices incorporating solution-processable metal nanoparticles, Appl. Phys. Lett. 95 (2009) 013305.
[57] O. Oklobia, T.S. Shafai, A quantitative study of the formation of PCBM clusters upon thermal annealing of P3HT/PCBM bulk heterojunction solar cell, Sol. Energy Mater. Sol. Cells 117 (2013) 1–8.
[58] P.K. Jain, K.S. Lee, I.H. El-Sayed, M.A. El-Sayed, Calculated absorption and scattering properties of gold nanoparticles of different size, shape, and composition: applications in biological imaging and biomedicine, J. Phys. Chem. B 110 (2006) 7238–7248.